Supplementary Material

S1 Aerodynamic resistance in the surface layer

S1.1 Aerodynamic resistance over Harvard Forest

Turbulent vertical transport of scalars within the atmospheric surface layer, often described as the lowest 10 % of the planetary boundary layer where fluxes of momentum, heat, and mass are assumed to be constant with height, is an important process governing surface-atmosphere exchange. Aerodynamic resistance to turbulent transport, most commonly parameterized in CTMs following Eq. (3), can take on a large range of values depending on the state of surface layer turbulence. Cumulative distributions of hourly values of R_a computed over Harvard Forest (June–November 2000) following parameterizations P1–P4 using MERRA-2 assimilated meteorology are depicted in Fig. S1 for two reference heights, 29 m and 60 m. Also depicted is R_a inferred from measured horizontal wind and friction velocity ($u*$) at 29 m, $R_a(29m) = u(29m)/u*^2$, assuming a no-slip boundary condition, i.e., $u(z_o) = 0$ m s^{-1}. Computed from the center of the lowest level in GEOS-Chem, P1 $R_a(60\ m)$ ranges from ~ 6 s m^{-1} (5th percentile) to ~ 400 s m^{-1} (95th percentile) with 50th percentile $R_a(60m)$ ~ 18 s m^{-1}. Thus, R_a has variable influence to total resistance represented through V_d, ranging from minor under well mixed conditions for species with substantial R_c, i.e., O_3 (Massman, 1994), HCN (Nguyen et al., 2015), and NO_2 (herein), to significant for species with negligible R_c under typical diabatic conditions, i.e., HNO_3 (herein), to dominant under conditions of very high stability and intermittent turbulence (Toyota et al., 2016).

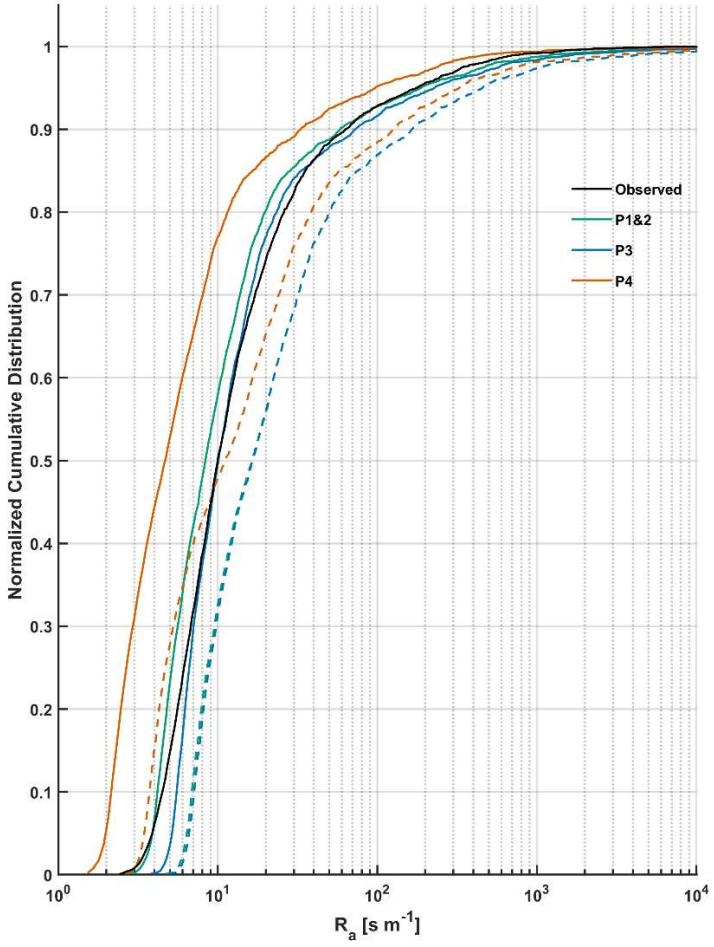

Figure S1: Cumulative distributions of hourly aerodynamic resistance R_a over Harvard Forest from June–November 2000. Measurement-inferred $R_a(29\ m) = u(29\ m)/u*^2$ is compared to coincidently sampled (hourly) simulated values P1&2, P3, and P4 integrated from both the 29 m measurement height at Harvard Forest (**solid lines**) and the approximate midpoint of GEOS-Chem's first level, ~ 60 m (**dashed lines**).

S1.2 Formulation of R_a from eddy diffusivity K_c

An equivalent formulation of R_a to that of Eq. (3) may be expressed as a vertical integration of eddy diffusivity K_c (Garratt, 1992):

$$R_a = \int_{z_o}^{z-d} \frac{1}{K_c(z)}\, dz\,, \tag{S1}$$

K_c is the eddy diffusivity for scalar quantities which is commonly represented as the product of characteristic surface layer scaling parameters u_* and height z above the displacement height (d) (Kaimal and Finnigan, 1994), corrected for non-neutral conditions via an empirically determined dimensionless flux–gradient relation for sensible heat ϕ_h commonly used interchangeably for scalar quantities:

$$K_c = \frac{u_* k(z-d)}{\phi_h(\zeta)}, \tag{S2}$$

where k = 0.4 is the von Karman constant, ϕ_h is an empirical function of the dimensionless M–O stability parameter $\zeta = (z - d) / L$, where L is the M–O length (Monin and Obukhov, 1954). Figure S2 includes calculated values of K_c following Eq. (S2), integrand of Eq. (S1) K_c^{-1}, and resulting R_a following Eq. (S1) as a function of height above ground over a rough surface under neutrally stable conditions.

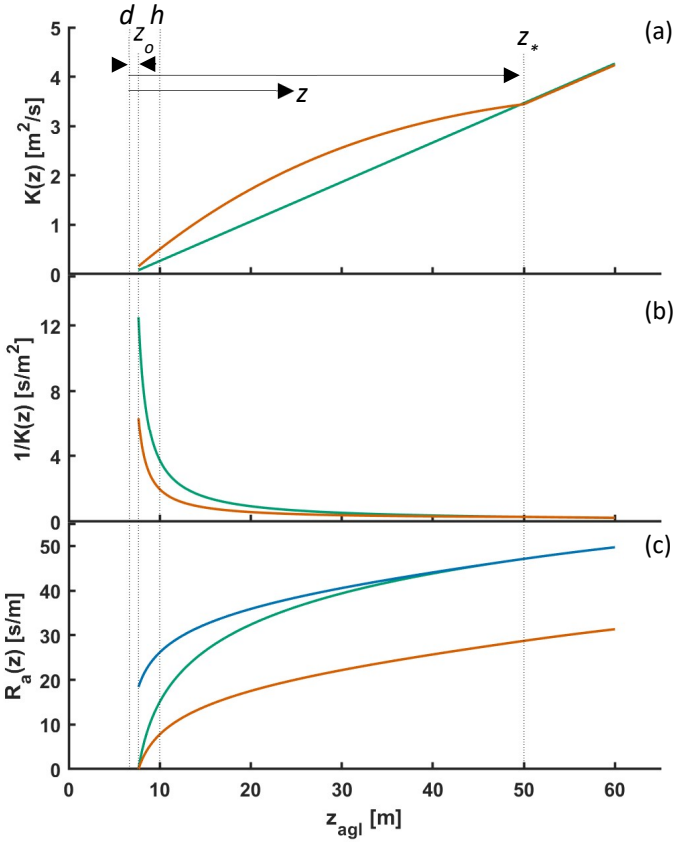

Figure S2: (a) Turbulent eddy diffusivity *K(z)* above a rough surface (z_o = 1 m) computed via standard Monin–Obukhov similarity theory according to Eq. (S2) (**green**) and using a perturbed Monin–Obukhov form (Eq. (S8)) to account for enhanced mixing within the roughness sublayer (**orange**). **(b)** $K(z)^{-1}$ depicts the integrand of corresponding aerodynamic resistance calculations (Eq. (S1)). **(c)** Aerodynamic resistance $R_a(z)$ computed following Eq. (S1) with stability correction functions according to M–O similarity theory (**green**) and a roughness sublayer perturbed from (Eq. (S8)) (**orange**), both of which assume zero wind at the roughness length z_o. $R_a(z)$ which accounts for both enhanced roughness sublayer mixing and non-zero wind at z_o is depicted in **blue** according to (Eq. S10). Meteorological conditions are taken as light winds (u_* = 0.2 m s^{-1}) and a neutrally stable atmosphere ($L^{-1} \sim 0$ m^{-1}).

S1.3 Monin–Obukhov (M–O) stability correction functions used in GEOS-Chem

Empirically determined dimensionless flux–gradient relations, also known as M–O stability correction functions, used to compute surface layer R_a in GEOS-Chem have the following functional (ϕ_h) and integral (Ψ_h) forms:

Unstable conditions ($\zeta < 0$) (Garratt, 1992; Holtslag et al., 1990)

$$\phi_h = (1 - 15\,\zeta)^{-1/2}\,, \tag{S3}$$

$$\Psi_h = 2\ln\left[\frac{1+\phi_h^{-1}}{2}\right], \tag{S4}$$

Stable conditions ($0 < \zeta \leq 1$) (Dyer, 1974)

$$\phi_h = 1 + 5\zeta\,, \tag{S5}$$

Stable conditions ($1 < \zeta$) (Holtslag et al., 1990)

$$\phi_h = 5 + \zeta\,, \tag{S6}$$

Stable conditions ($0 < \zeta$) (Holtslag and Bruin, 1988)

$$\Psi_h = -\left[a\zeta + b\left(\zeta - \frac{c}{d}\right)e^{-d\,\zeta} + \frac{bc}{d}\right], \tag{S7}$$

where a = 0.7, b = 0.75, c = 5, and d = 0.35.

S1.4 Roughness sublayer (RSL) mixing

Within a distance of 2 to 3 times the canopy height (h_c) above the surface, the so called roughness sublayer (RSL), turbulent eddy structure is significantly different from that of the remaining surface layer above (Finnigan et al., 2009; Raupach et al., 1996). Turbulent flows in the wake of roughness elements are dominated by structures of a larger length scale than predicted by Eq. (S2) where turbulent eddies are parameterized to scale on a distance z above d (Finnigan, 2000). Near the canopy top, K_c is enhanced over that predicted by M–O similarity theory by a factor of 2 to 3 (Cellier and Brunet, 1992; Raupach et al., 1996), approaching equivalence by ~ $2h_c$ (Simpson et al., 1998). To avoid underestimating turbulent transport of momentum, heat, and mass, models that employ gradient transport theory (K-theory) may scale eddy diffusivities within the RSL to values above those predicted by M–O similarity theory (Bryan et al., 2012; Mölder et al., 1999; Neirynck and Ceulemans, 2008; Sellers et al., 1986; Stroud et al., 2005). RSL functions $\widehat{\phi_x}$ designed as perturbations to the dimensionless universal M–O functions $\phi_x(\zeta)$ can be applied in multiplicative form, yielding modified M–O stability functions Φ_x:

$$\Phi_x = \phi_x(\zeta)\,\widehat{\phi_x}\,, \tag{S8}$$

where x refers to either momentum, heat, or scalar quantities. Several RSL functional forms have been proposed of varying complexity, all of which contain an additional RSL length scale, i.e., z^* in Eq. (S9). Computing mean wind and scalar profiles requires integral forms of corresponding non-dimensional M–O stability functions (Panofsky, 1963); some RSL modified M–O stability functions have analytical solutions to integral forms (Arnqvist and Bergström, 2015; de Ridder, 2010), while others require numerical integration (Cellier and Brunet, 1992; Garratt, 1980; Harman and Finnigan, 2007; Mölder et al., 1999; Wenzel et al., 1997). Physick and Garratt (1995) implement a simple RSL lower boundary correction into a mesoscale model using the RSL function:

$$\widehat{\phi_M} = \widehat{\phi_h} = 0.5 \exp\left[0.7\,\frac{(z-d)}{(z^*-d)}\right], \quad \text{(S9)}$$

where the RSL correction is treated the same for both momentum $\widehat{\phi_M}$ and sensible heat $\widehat{\phi_h}$ and is independent of buoyancy. Following Eq. (S9), turbulent mixing within the upper canopy at d is enhanced 2-fold, with $\widehat{\phi_M}$ and $\widehat{\phi_h}$ decaying to unity at the top of the RSL, z^*. The depth of the RSL was estimated following Physick and Garratt (1995); briefly, for neutral and unstable conditions ($L^{-1} \leq 0$), $z_N^* = 50\ z_o$; for very stable conditions ($z_N^* / L > 0.2$), $z^* = 0.37\ z_N^*$; for moderately stable conditions ($0 < z_N^* / L < 0.2$), z^* is linearly interpolated between neutral and stable values. It is noted that the additional mixing in the wake of roughness elements within the RSL reduces vertical gradients from those of M–O adjusted logarithmic values extrapolated from above the RSL; as such, flux–gradient wind profiles adjusted for stability and RSL effects can no longer be integrated assuming $u(z_o) = 0$ for $z < z^*$. An updated formulation of R_a which accounts for RSL effects and $u(z_o) > 0$ can be expressed as (Physick and Garratt, 1995):

$$R_a(z < z^*) = \frac{1}{k u_*}\left[\ln\left(\frac{z-d}{z_o}\right) - \Psi_h\left(\frac{z-d}{L}\right) + \Psi_h\left(\frac{z_o}{L}\right) + \int_z^{z^*} \phi_h\left(1 - \widehat{\phi_h}\right) z^{-1} dz\right], \quad \text{(S10)}$$

At the top of the RSL where $z = z^*$ and $\widehat{\phi_h} \sim 1$, R_a from Eq. (3) & Eq. (S10) become equivalent. Above the RSL ($z > z^*$) M–O similarity theory applies and R_a follows Eq. (3).

Included in Fig. S2 is a depiction of the effects of enhanced RSL mixing on K_c and R_a as a function of reference height z above the displacement height d for a rough surface (z_o = 1 m) under neutral stability conditions ($L^{-1} \sim 0$) and light winds (u_* = 0.2 m s^{-1}). K_c and K_c^{-1} calculated using the RSL modified M–O stability function Φ_x from Eq. (S9) are shown as orange traces in panels (a) and (b) of Fig. S2, respectively, and are compared to values from M–O similarity theory which neglects RSL effects (green trace). The largest relative difference in RSL-corrected K_c occurs at z_o, where the effect of Eq. (S9) is largest. Panel (c) in Fig. S2 includes $R_a(z)$ computed following M–O similarity theory (Eq. (3), green trace) alongside $R_a(z)$ according to Eq. (S10) (blue trace); the integral in Eq. (S10) was evaluated numerically via Simpson's method. Enhanced RSL mixing results in a weaker above-canopy vertical gradient in R_a, while allowing $u(z_o) > 0$ via Eq. (S10) results in a large displacement of $R_a(z_o)$. R_a following Eq. (3) and Eq. (S10) asymptotically converge to equivalency by $z = z^*$, with good and excellent agreement by $z = 2h_c$ (10 %) and $z = 3h_c$ (3 %), respectively, under these neutral test conditions. Reduced gradients in R_a with height results from growth of turbulent eddies (K_c) according to mixing length z - d. As previously noted, R_a computed from integration of K_c^{-1} (Eq. (S2)) where K_c is corrected for buoyancy following ϕ_h is equivalent to R_a computed following Eq. (3), both being depicted in panel (c) of Fig. S2 (green trace). However, integration of K_c^{-1} where K_c is corrected for buoyancy and RSL effects following the modified M–O stability correction $\widehat{\phi_h}$ is not equivalent to RSL R_a computed following Eq. (S10), as seen in Fig. S2c (red trace), as the former assumes $u(z_o) = 0$ and the later $u(z_o) > 0$. Although the vertical gradients of these two methods are identical, R_a corrected for the RSL following Eq. (S10) is shifted by $R_a(z_o)$.

It is noted that RSL-corrected R_a has directional asymmetry, where aerodynamic resistance to upward transport of surface emissions (orange trace in Figs. S1 & S2) is significantly less than aerodynamic resistance to dry deposition (blue trace in Figs. S1 & S2). This directional asymmetry is intuitive, as resistance to upward mixing of surface emissions would not be impeded, but enhanced, by non-zero wind at z_o, whereas dry deposition of uniformly mixed trace species from aloft requires contact with surface elements for removal. It is also noted that many efforts to simulate bidirectional surface exchange of atmospheric trace species employ R_a following standard M–O similarity theory according to Eq. (3) for both emission and deposition pathways (Haghighi and Or, 2015; Karamchandani et al., 2015; Nemitz et al., 2000; Su et al., 2011; Wen et al., 2014; Wentworth et al., 2014), thus failing to account for directional asymmetry in resulting fluxes. To prevent the underestimation of upward sensible and latent heat fluxes, Sellers et al. (1986) in their formulation of a Simple Biosphere Model (SiB) for use in General Circulation Models (GCMs) impose an aerodynamic resistance to emission from an integration of a RSL modified K_h, which would be similar to that depicted

in Fig. S2c (red trace). In Boys et al. (in prep), directional asymmetry of R_a is implemented into a simple model of subgrid dry deposition of near-surface emitted NO_x.

S2 Review of reactive uptake coefficients for NO_2 to hydrated surfaces

Although the mechanism for heterogenous hydrolysis of NO_2 (reaction R1 in main text), likely involving disproportionation of N_2O_4 as a surface intermediate (Finlayson-Pitts et al., 2003), is still an active area of research (Bang et al., 2015; Finlayson-Pitts, 2009; Murdachaew et al., 2012; Spataro and Ianniello, 2014), uptake coefficients for NO_2 (γ_{NO_2}) to various surfaces have been measured. Laboratory determined values of γ_{NO_2} are generally in the range of 10^{-7} to 10^{-5} for humidified and aqueous surfaces of various composition (Ammann et al., 2005; Bröske et al., 2003; Kleffmann et al., 1998; Kurtenbach et al., 2001), however, values > 10^{-5} (Mertes and Wahner, 1995; Msibi et al., 1993) and < 10^{-8} (Ammann et al., 2013) to bulk liquid water have been reported. Studies finding slow uptake of NO_2 to bulk water understand the process as driven by low solubility and slow aqueous phase second-order hydrolysis (Cheung et al., 2000; Lee and Schwartz, 1981; Schwartz and Lee, 1995), while studies finding uptake above that which can be accounted for by these solution-phase processes suggest heterogeneous first-order hydrolysis at the air–water interface (Bambauer et al., 1994; Finlayson-Pitts et al., 2003; Mertes and Wahner, 1995; Novakov, 1995). Recent efforts to understand the orders of magnitude variation in laboratory determined γ_{NO_2} to aqueous surfaces have employed electrospray ionization (ESI) mass spectrometry (MS) to monitor online NO_3^- formation from the reaction of $NO_{2(g)}$ injected into the ESI source region with aqueous electrosprays containing various concentrations of atmospherically relevant solutes, finding large enhancements in inferred γ_{NO_2} of up to a factor of 10^4 to solutions containing halide salts NaX (X = Cl, Br, I) (Colussi and Enami, 2019; Kinugawa et al., 2011; Yabushita et al., 2009). It was proposed that interfacial anions (Cl^-, Br^-, I^-) stabilize NO_2 at the air–water interface, facilitating heterogeneous hydrolysis. To this end, it was noted that Bambauer et al. (1994) reported enhanced uptake of NO_2 to aqueous droplets containing ~ 3 mM NaCl; however, Msibi et al. (1993) reported a value for γ_{NO_2} to deionized water of 8.7 x 10^{-5}—much greater than can be accounted for by dissolution followed by second-order hydrolysis, i.e., γ_{NO_2}~ 6 x 10^{-9} (Ammann et al., 2013). Due to the unique complexity of the ESI process, further work is required before application of these results to atmospherically relevant interfacial surfaces (Gallo et al., 2019b, 2019a; Rovelli et al., 2020). Additionally, the presence of reducing solutes such as ascorbic acid (Msibi et al., 1993) and phenolic humic acid precursor molecules (Ammann et al., 2005) have been shown to significantly enhance NO_2 surface uptake via one-electron reduction reactions yielding nitrate/HONO, and may also contribute to NO_2 deposition within the interior of leaves (Farvardin et al., 2020).

For use in models of atmospheric chemistry, field–measured γ_{NO_2} have provided some constraint on the large variation in laboratory determined values. Kurtenbach et al. (2001) studied heterogeneous HONO formation in a road traffic tunnel in Wuppertal, Germany, and found γ_{NO_2} ~ 10^{-6} to a sample of tunnel wall residue to be in good agreement with first-order heterogeneous formation rates of HONO from the tunnel experiments. VandenBoer et al. (2013) report high resolution vertical profiles (10 m resolution to 250 m AGL; < 10 min/profile) of various trace species including HONO and NO_2 at the Boulder Atmospheric Observatory (BAO) in Colorado, U.S. during late winter of 2011. The BAO site was situated in an agricultural region 32 km northeast of Boulder and was decommissioned in 2018 (Wolfe, 2018). VandenBoer et al. (2013) derived ground uptake coefficients for NO_2 ($\gamma_{NO_2,\ ground}$) by assuming the column integrated rate of change of HONO during the first half of the night (1800–2400) when HONO was increasing from very low daytime concentrations (mid-day photolysis lifetime of HONO < 15 minutes) was due to heterogeneous hydrolysis of NO_2 occurring on ground surfaces, and found $\gamma_{NO_2,\ ground}$ to vary between 2 x 10^{-6} and 1.6 x 10^{-5} as a function of RH for the specific wintertime land type in the vicinity of the BAO site (grassland and tilled

fields). Ren et al. (2020) monitor NO_2 and HONO concentrations at high temporal resolution at a meadow location (grass height ~ 30 cm, LAI ~ 6) in Melpitz, Germany, and similarly compute NO_2 uptake coefficients due to reaction R1 during early evening when HONO is accumulating in the nocturnal boundary layer, finding γ_{NO_2} = 2.3 ± 1.9 x 10^{-6}. Collins et al. (2018) found γ_{NO_2}= (1–2.3) x 10^{-6} from NO_2 decay, presumably via reaction R1, following indoor (residential) perturbation experiments probing the gas–surface equilibrium control over HONO concentrations for which surfaces have developed sufficient reservoirs of HONO/nitrite via heterogeneous reaction of NO_2 and by deposition of HONO emitted during operation of a gas stove.

S3 Parameterization of soil NO canopy reduction factor (CRF) in GEOS-Chem

Within-canopy NO_x loss processes removing up to 70–80 % of soil-emitted NO in mature forest ecosystems have been required to reconcile measured soil NO emissions with above-canopy NO_x observations (Jacob and Wofsy, 1990; Lerdau et al., 2000; Min et al., 2014). Emitted from soils as NO and deposited within canopies as NO_2, deposition-based parameterizations of soil NO canopy reduction factors (CRF) for use in large-scale CTMs yield global mean reductions in above-canopy soil NO_x fluxes from ~ 20 % (Wang et al., 1998) to 50 % (Yienger and Levy, 1995). Soil NO in GEOS-Chem follows the Berkeley–Dalhousie Soil NO_x Parameterization (Hudman et al., 2012), with a CRF as implemented by Wang et al. (1998):

$$CRF = \frac{k_d}{k_v + k_d}, \tag{S11}$$

where k_v [m s^{-1}] is the canopy air ventilation coefficient (Martens et al., 2004; Trumbore et al., 1990) and k_d [m s^{-1}] the deposition coefficient for NO_2 in canopy air. k_v is an empirical function of land type, surface wind speed, and LAI and is tuned to yield canopy air residence times for soil-emitted inert tracers in the Amazon Rainforest of 1 h during daytime and 5 h at night (Jacob and Wofsy, 1990). Nocturnal canopy air residence times on the order of 2–10 h for the Amazon Rainforest have been estimated from in-canopy measurements of soil-emitted ^{222}Rn (Martens et al., 2004; Trumbore et al., 1990). Application of k_v to additional land types in GEOS-Chem follows:

$$k_v = k_v^{RF} \sqrt{\frac{u^2}{9} \frac{7}{LAI}} \frac{\gamma^{RF}}{\gamma}, \tag{S12}$$

where u is the wind speed 10 m above the displacement height, k_v^{RF} is the canopy air ventilation coefficient tuned for the Amazon Rainforest (LAI = 7, u = 3 m s^{-1}) with daytime and nighttime values of 1x10^{-2} m s^{-1} and 2x10^{-3} m s^{-1}, respectively, and γ a nondimensional extinction coefficient for in-canopy wind speed with a value of 4 for both rainforest and temperate forest ecosystems (Wang et al., 1998). The deposition coefficient k_d in GEOS-Chem is taken as $R_c(NO_2)^{-1}$. Hudman et al. (2012) find that this representation of the CRF in GEOS-Chem results in a 16 % global reduction in above-canopy soil NO emission. Herein we compute the CRF following Eqs. (S11–S12) using site specific meteorology and canopy parameters. We set $k_d = [(R_c(NO_2)^{-1} + R_{chem}(NO_2 \rightarrow N_2O_5)^{-1}]$, where in addition to canopy uptake as described through $R_c(NO_2)$, we include an estimate of the minimum canopy resistance to nocturnal chemical loss of NO_2, $R_{chem}(NO_2 \rightarrow N_2O_5)$ = V_{chem}^{-1} ~ 2000 s m^{-1}. We note that k_d following this approach assumes that soil NO is oxidized to NO_2 on a much shorter timescale (minutes) than nocturnal vertical mixing of ground-level air parcels—a reasonable assumption given that: (i) nocturnal in-canopy O_3 concentrations of 10–25 ppb are much greater than NO concentrations at this site (Horii et al., 2004; Munger et al., 1996) and (ii) air parcel residence times for stable evening/nighttime conditions are on the order of tens of minutes to hours in the lower canopy of mature forests (Bannister et al., 2022; Martens et al., 2004; Trumbore et al., 1990). Recent observations of daytime air parcel residence times in mature forest canopies are on the order of tens of seconds to a few minutes (Bannister et al., 2022; Martens et al., 2004)—much

less than 1 h to which daytime k_v^{RF} in Eq. (S12) is tuned. Although beyond the scope of this work, updating the parameterization of k_v in GEOS-Chem to yield more realistic daytime canopy air residence times (Gerken et al., 2017) seems warranted. Such reductions in simulated daytime canopy air residence times would result in commensurate reductions to the CRF in Eq. (S11) due to reduced time for deposition of NO_2 prior to ventilation; however, incorporation of canopy NO_x chemistry into the CRF parameterization could partially offset these reductions (Delaria and Cohen, 2020; Min et al., 2014). Given the nocturnal focus of this study, we proceed with using the CRF parameterization from GEOS-Chem, modified to include nocturnal chemical loss of NO_2 in addition to deposition, as previously discussed.

As seen in the bottom panel of Fig. S3, the CRF from the base simulation P1 results in canopy-top soil NO reductions of 30 % at night, increasing slightly to 35 % during the day at the location of Harvard Forest over the period April–November. This weak diel behavior results from a similar day-to-night reduction in both k_d and k_v of more than an order of magnitude (Fig. S6 includes diel $R_c(NO_2)$ at the HFEMS). The reversal of the CRF diel pattern seen in updated parameterizations P6–P8 reflect the large increases in simulated surface uptake of NO_2 at night through implementation of reaction R1 via dry deposition, discussed in Section 3.3.3.

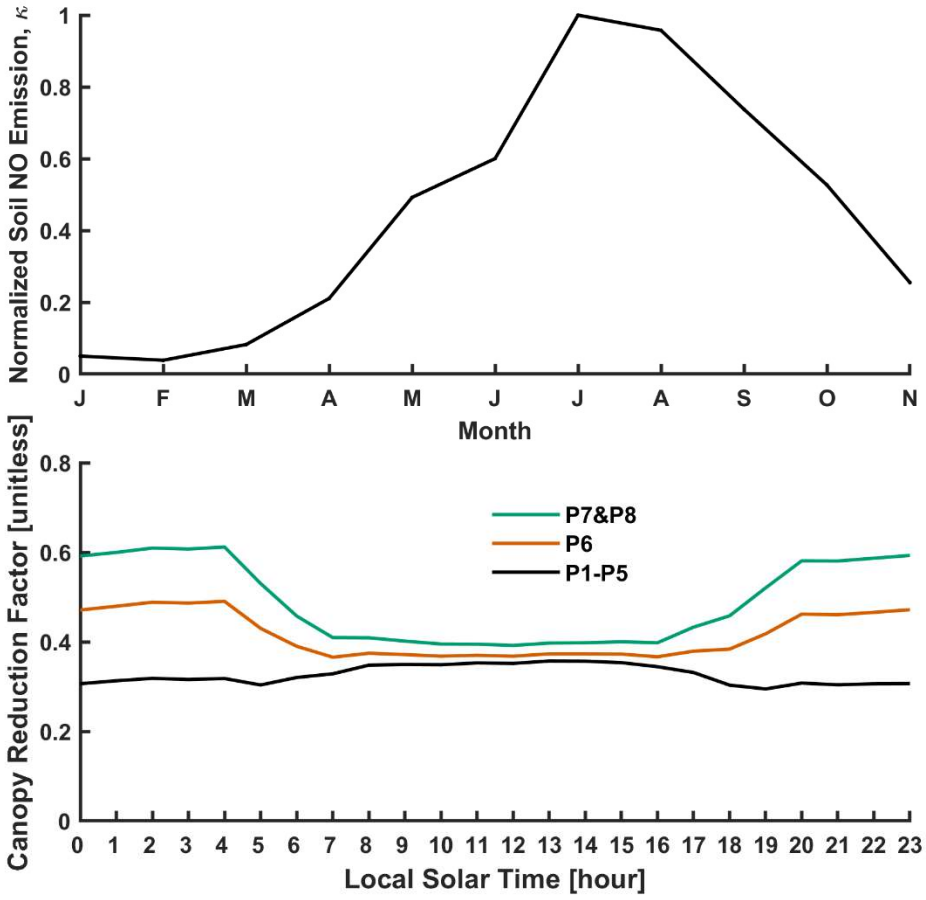

Figure S3: (**TOP**) Normalized monthly nocturnal soil NO emission simulated from GEOS-Chem at the location of Harvard Forest. (**BOTTOM**) Diel climatology (April, July–November) of the soil NO canopy reduction factor (Eq. (S11)) for parameterizations P1–P5, P6, and P7 & P8.

S4 Review of nocturnal stomatal behavior

Stomatal pores exist in leaves to optimize plant water-use-efficiency—the number of molecules of H_2O transpired per molecule of CO_2 fixed via photosynthesis. Stomatal aperture is under guard cell regulation in response to environmental conditions such as solar radiation, guard cell CO_2 concentration, soil moisture, water vapor pressure deficit (VPD), and temperature (Costa et al., 2015; Nobel, 2009). Fully open stomata occupy ~ 0.2–2 % of leaf surface area, with a density of ~ 50–300 stomata per mm^2 on the stomata containing surfaces of leaves of temperate terrestrial plants, making available a moist interior leaf surface area to photosynthetic mesophyll cells that is in the range of 10–50 times larger than the projected leaf area (i.e., LAI) (Nobel, 2009; Nobel et al., 1975).

Both canopy-scale and leaf-level observations of trace gas uptake attempt to separate stomatal from non-stomatal pathways. A simple approach is to assign nocturnal/dark uptake as entirely non-stomatal, dependent on the assumption of stomatal closure. In addition to darkness, chamber studies may introduce other stimuli known to reduce stomatal aperture, such as water stress, elevated CO_2, or the plant hormone abscisic acid (ABA) (Chaparro-Suarez et al., 2011; Costa et al., 2015; Delaria et al., 2020). Trace gas specific stomatal conductance (g_{sx}) may be deduced by scaling stomatal conductance to water vapor (g_s)—inferred in chamber studies by normalizing measured water vapor flux by leaf VPD (Delaria et al., 2020; Thoene et al., 1996; Wang et al., 2020), and in canopy-scale studies by inversion of the Penman–Monteith equation using above-canopy water vapor flux (Lamaud et al., 2009)—by the ratio of diffusivities D_x/D_{H_2O} in air. Estimates of stomatal conductance enable separation of non-stomatal from stomatal uptake—including estimates of mesophilic resistance to the leaf interior—by non-linear fits to plots of $V_d(x)$ vs g_{sx} (Delaria et al., 2020). However, this method assumes that the measured evaporative flux is due entirely to gaseous diffusion of water vapor through stomatal pores, without contribution from other sources including evaporation from soil or moisture that may be present on canopy elements as a result of precipitation, dew, or elevated humidity. Significant scatter and elevated values in inferred g_s have been noted at the canopy scale for RH > 60 % and for a period of time (days) following rainfall, motivating efforts to fit relations of g_s to CO_2 assimilation flux (which assume nocturnal stomatal closure) on ideal days for application across all conditions of canopy moisture (Lamaud et al., 2009; Plake et al., 2015; Stella et al., 2013).

In addition to the challenge of measuring stomatal conductance under elevated RH, mounting evidence exists for the presence of thin aqueous films on foliar surfaces at ambient humidities well below saturation, resulting from the deliquescence of deposited hygroscopic material in the high humidity laminar boundary layer of transpiring leaves (Burkhardt et al., 1999, 2001a; Burkhardt and Gerchau, 1994; Burkhardt and Hunsche, 2013; Grantz et al., 2018). Concentrated solutions of deliquesced material have sufficiently low surface tension to spread over hydrophobic leaf cuticles and penetrate stomatal pores as thin liquid films (< 100 nm thick), connecting to apoplastic liquid water within the leaf interior—a process known as 'hydraulic activation of stomata' (HAS) (Burkhardt, 2010). An osmotic gradient in water potential drives water movement through hydraulically activated stomata to the leaf exterior, where evaporation occurs uncoupled from stomatal aperture—a process known as 'wicking'. This additional pathway for water efflux escapes stomatal regulation, thereby reducing plant water-use-efficiency and drought tolerance. Significant increases in minimum cuticular conductance to water on the order of 23–30 % have been noted across coniferous and deciduous tree species for foliage exposed to ambient air (ionic aerosol concentration of 4.9 μg m^{-3}) compared to filtered air (ionic aerosol concentration of 0.67 μg m^{-3}) (Burkhardt et al., 2018). Similar experiments conducted on shorter lived faba beans (*Vicia faba*) noted significant increases in both minimum cuticular conductance (16 % average, 80 % max) and nocturnal stomatal conductance (~ 40 %) (Grantz et al., 2018). Foliar exposure studies to higher concentrations of hygroscopic aerosol have found large increases in nocturnal stomatal conductance (80–90 %) when stomatal aperture was at a minimum, decreasing to less than 30 % for (i) fully open stomata when water vapor dominates transpiration (Burkhardt et al., 2001b) and (ii) 7 h post exposure, presumably due to stomatal uptake of dissolved ions through thin aqueous films (Motai et al., 2018)—the latter indicating that

wicking via HAS requires continuous deposition of hygroscopic material to leaf cuticles in order to maintain a sufficient osmotic gradient. Cuticle loads of hygroscopic material of up to 50 μg cm^{-2} in these exposure studies were in the range found on urban trees (Burkhardt, 2010).

Considering the evidence for a liquid phase water loss pathway via HAS on plants exposed to moderate levels of hygroscopic aerosol, overprediction of stomatal conductance may exist in studies conducted near developed environments, especially under dark conditions when stomatal aperture is at a minimum and wicking from HAS therefore a larger relative fraction of total foliar water loss. Chamber studies may be particularly susceptible to this overprediction given the mechanically mixed conditions often used to minimize diffusive boundary layer resistances (Burkhardt et al., 2001b; Pariyar et al., 2013), thereby confounding partitioning of non-stomatal and stomatal deposition pathways under dark conditions from scaled estimates of stomatal conductance to water vapor.

Surface area also plays an important role in trace gas uptake within the interior of leaves. Nobel et al. (1975) found that a 4-fold increase in CO_2 uptake between shade and sun leaves of the deciduous species 'Creeping Charlie' (*Plectranthus parviflorus*) could be explained by the corresponding increase in mesophyll cell surface area per unit LAI (A^{mes}/LAI), and that internal leaf resistance to CO_2 per unit area of mesophyll (A^{mes}) remained constant. To our knowledge, no such analysis has been conducted for foliar uptake of NO_2. Delaria et al. (2020) provide estimates of mesophilic resistance (r_m) for NO_2 to six coniferous and four deciduous tree species native to California, with values of r_m ranging from 20–130 s m^{-1} (median 48 s m^{-1}, mean 57 s m^{-1}) per unit LAI, which at the forest canopy scale would represent a small (< 5 %) and modest (~ 15 %) fraction of bulk-canopy $R_c(NO_2)$ for nighttime and daytime conditions at Harvard Forest, respectively, during summer (Fig. S6 & Table S3). Nonetheless, using the A^{mes}/LAI value of 50 corresponding to deciduous sun leaves from Nobel et al. (1975) and the NO_2 uptake coefficient to distilled water of 2.3 x 10^{-6} (Table 1), an estimate of r_m due to uptake on moist intercellular leaf surfaces is ~ 100 s m^{-1}. This suggests, on average, an additional pathway for NO_2 uptake to leaf interiors with a resistance on the order of 100 s m^{-1} is acting in parallel to reaction R1—a likely pathway being NO_2 scavenging by apoplastic antioxidants (Farvardin et al., 2020; Msibi et al., 1993; Ramge et al., 1993; Teklemariam and Sparks, 2006). The assumption that the ratio A^{mes}/LAI ~ 50 is representative and constant across the species examined by Delaria et al. (2020) is a generalized approximation and further work is required to understand the mechanisms driving intra- and interspecies variability in r_m. Future leaf-level study into the mechanism of foliar NO_2 uptake would benefit from consideration of possible HAS, A^{mes}/LAI, as well as apoplastic antioxidant concentrations.

Supplemental figures and tables

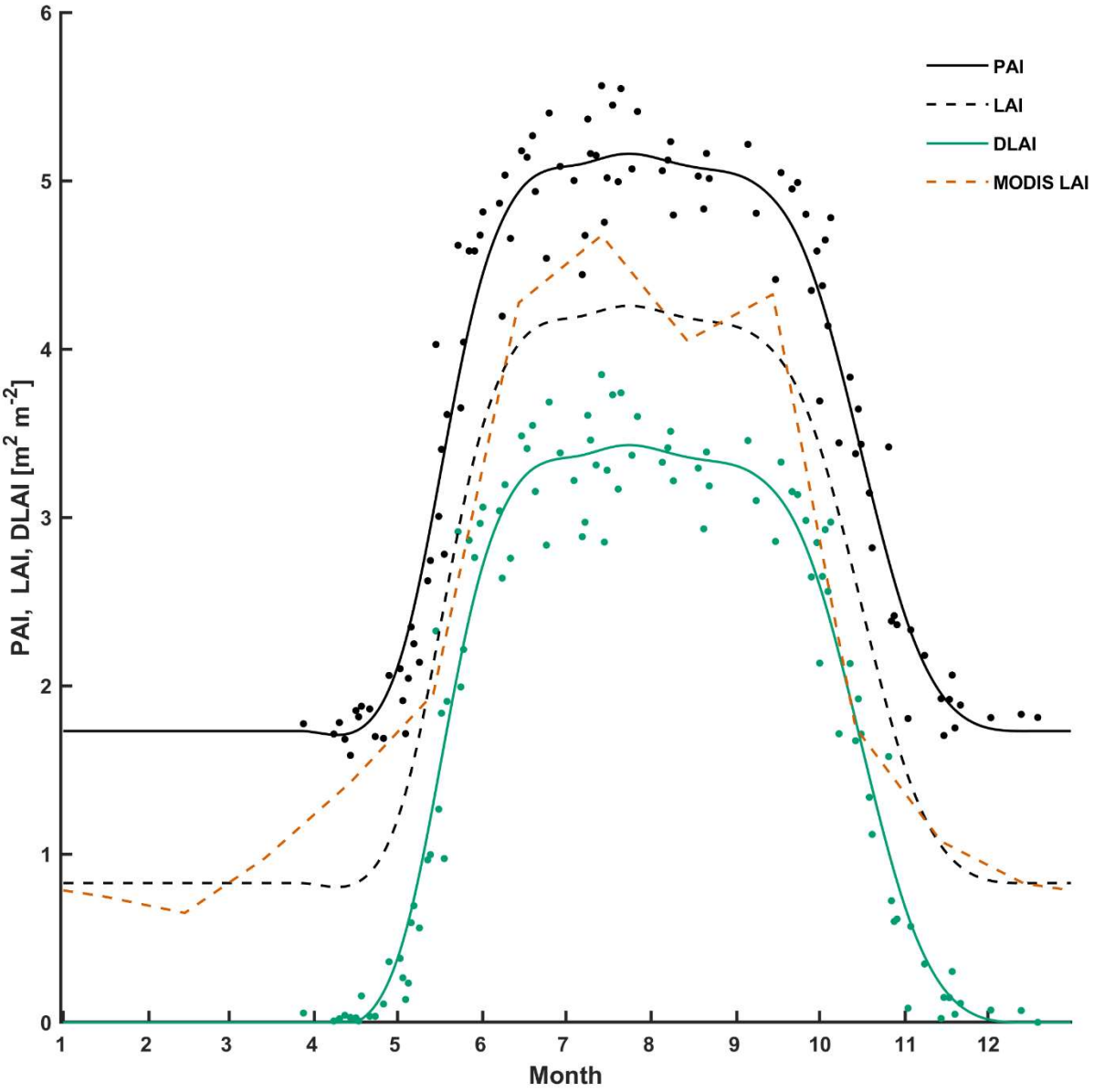

Figure S4: Observed plant area index (**PAI**) and deciduous leaf area index (**DLAI**) at Harvard Forest from 1998–2015. Leaf area index (**LAI**) includes both deciduous and coniferous foliage and is computed herein as a spline-fit to observed PAI corrected for reported stem and twig area index (STAI = 0.9). Also depicted is a multiyear mean (2005–2008) **MODIS LAI** for the corresponding 0.25° x 0.25° grid cell. Dots depict measurements of PAI and DLAI obtained from the Harvard Forest Data Archive (Matthes et al., 2024). STAI = 0.9 was reported by Horii et al. (2005).

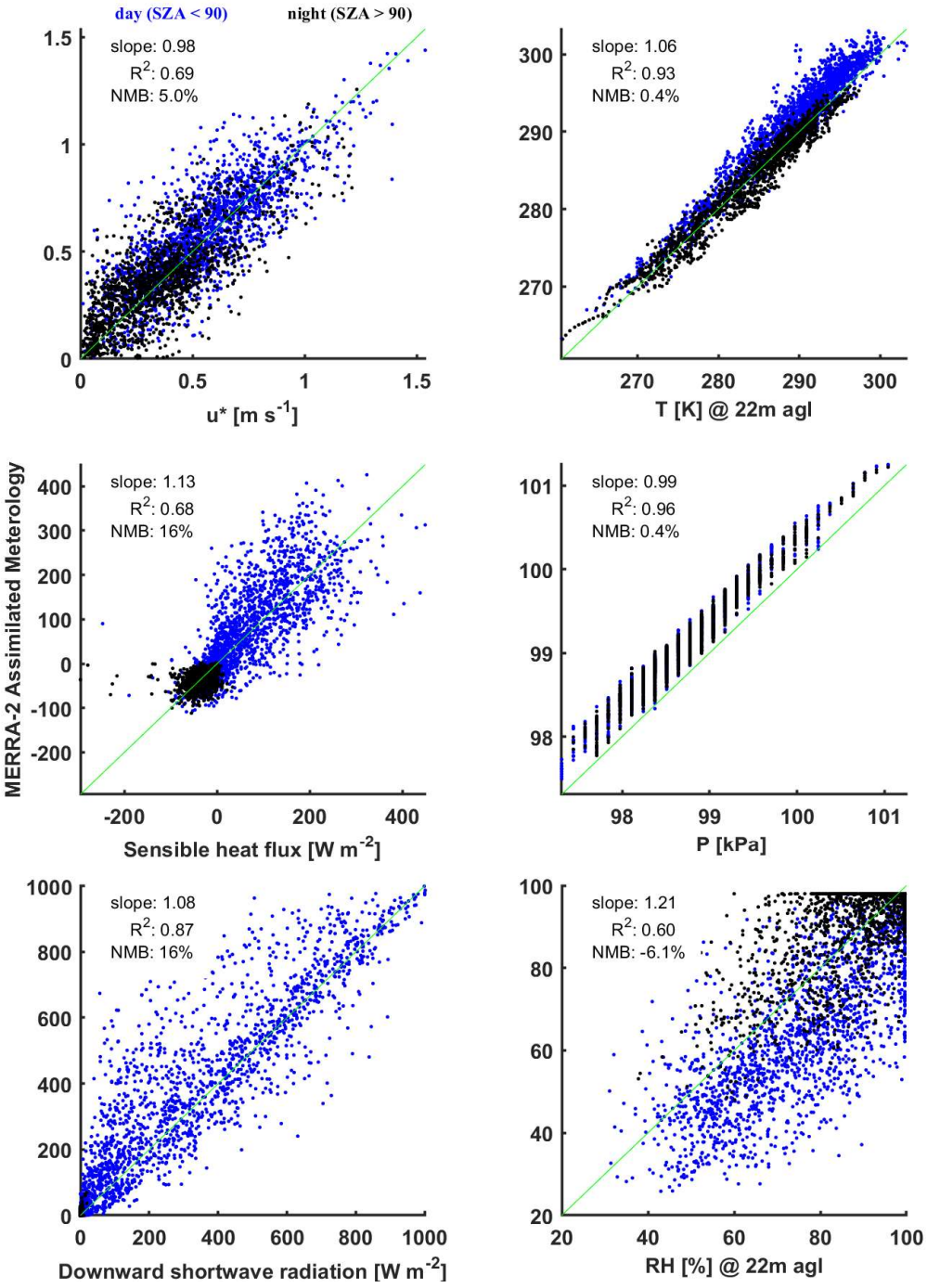

Figure S5: Comparisons of hourly observations of friction velocity u_*, sensible heat flux, downward shortwave radiation, *T*, *P*, and *RH*, made over Harvard Forest to coincident values from GEOS assimilated meteorological fields (MERRA2 @ 0.5˚ x 0.625˚). Daytime observations are shown for solar zenith angles SZA < 90° and nighttime for SZA > 90°. Striations in comparison of pressure result from measured values reported on 133 Pa intervals.

Table S1: Compilation of binary gas phase diffusion coefficients in air or N_2 for atmospherically relevant molecules. Computed values following the semi-empirical technique of Fuller's method are tabulated alongside measured values where available. Diffusivities (D_o) are reported at 273 K and 101 325 Pa following Eq. (6)**.**

Species	**Fuller's Method**	**Measured**		**Ref.**[(a)]
	D_o ($cm^2\ s^{-1}$)	D_o ($cm^2\ s^{-1}$)		
inorganics				
HNO_3	0.130	0.099	± 0.008	1
NO_3	0.142	0.105	± 0.053	1
HONO	0.151	0.110	± 0.03	1
NH_3	0.228	0.201	± 0.011	1
SO_2	0.115	0.107	± 0.015	1
H_2SO_4	0.094	0.085	± 0.011	1
H_2O_2	0.168	0.133	± 0.04	1
HOBr	0.115	0.096	± 0.01	1
HBr	0.127	0.109	± 0.033	1
HCl	0.148	0.135	± 0.008	1
Cl_2	0.106	0.107	± 0.011	1
I_2	0.083	0.061	± 0.015	1
Br_2	0.096	0.086	± 0.007	1
NO_2	0.157	0.145	± 0.001	2
N_2O_4	0.111	0.084	± 0.004	2
N_2O_5	0.103	0.081	± 0.005	2
$ClONO_2$	0.100	0.085	± 0.001	2
O_3	0.152	0.153	± 0.001	2
H_2O	0.229	0.218		3
CO_2	0.133	0.138		3
N_2O	0.164	0.144		3
CO	0.161	0.181		3
NO	0.199	0.180		3
organics				
methane	0.181	0.190	± 0.006	4
ethane	0.122	0.129	± 0.006	4
propane	0.097	0.098	± 0.006	4
ethylene	0.129	0.140	± 0.006	4
benzene	0.077	0.081	± 0.003	4
toluene	0.069	0.076	± 0.005	4
xylene	0.064	0.061	± 0.006	4
methanol	0.138	0.142	± 0.012	4
ethanol	0.106	0.111	± 0.008	4
acetone	0.091	0.092	± 0.006	4
methyl ethyl ketone	0.082	0.078	± 0.002	4
formic acid	0.125	0.131	± 0.005	4
acetic acid	0.100	0.106	± 0.006	4
peroxyacetyl nitrate	0.080	-		-
Hydroxymethyl hydroperoxide	0.107			
CCl_4	0.070	0.069	± 0.003	5
CH_2Cl_2	0.090	0.089	± 0.005	5
$CHCl_3$	0.078	0.078	± 0.003	5
$CHBr_3$	0.073	0.066	± 0.001	5

[(a)] References for measured diffusion coeficients:
(1) Tang et al. (2014)
(2) Langenberg et al. (2020)
(3) Massman (1998)
(4) Tang et al. (2015)
(5) Gu et al. (2018)

Table S2: Inferred NO_2 uptake coefficients γ_{NO_2} to both non-foliar and foliar materials from literature values of surface deposition velocities V_d^{surf}. Abbreviations used: Eddy Covariance (EC), Non-Stomatal (NS), Leaf Area Index (LAI), Table (T), Figure (F).

Material	Measurement Technique	V_d^{surf}	γ_{NO_2} [a]	Surface Area [b]	T	RH	Ref. [j]
	method/location/condition	[cm s^{-1}]	(unitless)		[°C]	[%]	
Non-Foliar Surfaces							
Teflon	chamber/ lab	~ 0	~ 0	total	29.4	unknown	1
distilled water	chamber/ lab	0.021	2.3 x 10^{-6}	total (planar)	29.4	N/A	1
concreate (fine)	chamber/ lab	0	0	geometric	22	30	2, T5
		0.01	1.1 x 10^{-6}			50	
		0.01	1.1 x 10^{-6}			90	
concrete (coarse)	chamber/ lab	0	0	geometric	22	30	2, T5
		0.02	2.2 x 10^{-6}			50	
		0.03	3.3 x 10^{-6}			70	
		0.03	3.3 x 10^{-6}			90	
wood board (untreated,	chamber/ lab	0	0	geometric	22	50	2, T5
hard, fine, aged)		0.007	7.6 x 10^{-7}			70	
		0.015	1.6 x 10^{-6}			90	
plywood (untreated)	chamber/ lab	0.013	1.4 x 10^{-6}	geometric	unknown [c]	50	2, T5
tree bark (wet)	chamber/ lab	0.093	1.0 x 10^{-5}	geometric	29.4	N/A	1
tree bark (dry)	chamber/ lab	0.047	5.0 x 10^{-6}	geometric	29.4	unknown	1
forest floor (hardwood)	chamber/ lab	0.47	5.0 x 10^{-5}	planar	29.4	unknown	1
forest floor (coniferous)	chamber/ lab	0.48	5.1 x 10^{-5}	planar			1
forest floor	chamber/ field	0.40	4.3 x 10^{-5}	planar	10 to 22	~60 ± 20	3
snow	EC/ prairie/ winter	0.14	1.6 x 10^{-5}	planar	-20 to 0	N/A	4 [d]
Foliar Surfaces							
White pine (Pinus strobus)	chamber/field/NS	0.043	4.6 x 10^{-6}	LAI	30	67	5
		0.016	1.7 x 10^{-6}	total leaf area [e]			
10 tree species: 6 conif., 4 decid.	chamber/ lab/dark				20	<90	6 [g]
Coniferous, avg. of 6 species		0.034 (0.009–0.087)	3.7 x 10^{-6}	LAI			6, T2 [h]
		0.013	1.4 x 10^{-6}	total leaf area [e]			
Deciduous, avg. of 4 species		0.017 (0.004–0.037)	1.9 x 10^{-6}	LAI			6, T2 [h]
		0.0090	9.8 x 10^{-7}	total leaf area [e,f]			
CA Oak (Quercus agrifolia)	chamber/ lab/ dark	0.015	1.6 x 10^{-6}	LAI	22	50–65	7

		0.0080	8.7 x 10^{-7}	total leaf area[e,f]			
5 tree species: 4 decid., 1 conif.	chamber/ lab/			"leaf area"			8[g]
avg. of 4 conif. species	abscisic acid	0.013 (0–0.025)	1.4 x 10^{-6}		20–25	50–60	8, F5[i]
avg. of all 5 species	dark	0.012 (0.004–0.021)	1.3 x 10^{-6}		20	50	8, F7[h]
2 conif. species: pine & spruce	chamber/ field/ dark	0.056 (0.03–0.08)	6.2 x 10^{-6}	LAI	10–14	50–70	3[g]
		0.021	2.3 x 10^{-6}	total leaf area[e]			
8 tree species: 3 conif., 5 decid.	chamber/ lab/				29.4	unknown	1
Coniferous, avg. of 3 species	dark (min g_s)	0.015 (0.003–0.03)	1.6 x 10^{-6}	total leaf area			1, F4[i]
Deciduous, avg. of 5 species	NS at g_s= 0	0.014	1.5 x 10^{-6}	LAI			1, T2[i]
		0.007	7.5 x 10^{-7}	total leaf area [e.f]			
Norway Spruce (Picea abies L.)	chamber/ field/ dark	0.014	1.5 x 10^{-6}	total leaf area	11.3±2.8	85.4±11.1	9, T2[i]
Deciduous leaves (average)		0.015	1.7 x 10^{-6}	LAI		50 to <90	1,6-8
Coniferous leaves (average)		0.041	4.6 x 10^{-6}	LAI		50 to <90	1,3,5,6,8,9
Coniferous leaves (average)		0.015	1.7 x 10^{-6}	total leaf area[e]		50 to <90	1,3,5,6,8,9

[a] Uptake coefficients for NO_2 inferred herein from literature values of surface deposition velocities: $\gamma_{NO_2} = 4\, v_d^{surf} \bar{v}_t^{-1}$, where $\bar{v}_t$ is the mean thermal speed of NO_2, and v_d^{surf} the material-specific deposition velocity measured from well-mixed (minimal $R_a + R_b$) chamber studies, with the exception of uptake to snow which was measured via the eddy covariance technique.

[b] Surface area used to normalize material-specific deposition fluxes in the computation of material-specific v_d^{surf}.

[c] Assume chamber temperature of 20 °C for calculating γ_{NO_2}.

[d] v_d^{surf} to snow was computed herein from reported eddy covariance (EC) inferred $R_c(NO_2)$ to snow of 740 ± 210 s m^{-1}.

[e] Reported v_d^{surf} normalized to LAI (projected leaf area) were scaled herein to reflect uptake to total leaf surface area—a factor of two for deciduous leaves and 2.7 for coniferous needles (see Section 2.4, Section 3.3.4, and Section 4).

[f] Non-stomatous adaxial (top) side of deciduous leaves may not have sufficient thin water films (Burkhardt et al., 1999) to support NO_2 uptake via hydrolysis.

[g] References which find stomatal conductance sufficient to explain observed NO_2 uptake under conditions of minimal stomatal aperture.

[h] Mean value averaged herein from values reported in indicated table or estimated from indicated figure (i.e., T2 = Table 2; F7 = Fig. 7) of reference.

[i] v_d^{surf} computed herein by normalizing reported (from Table) or estimated (from Figure) mean NO_2 flux by mean concentration.

[j] References for material-specific $v_d^{surf}(NO_2)$

(1) Hanson et al. (1989)
(2) Grøntoft and Raychaudhuri (2004)
(3) Rondón et al. (1993)
(4) Stocker et al. (1995)
(5) Wang et al. (2020)
(6) Delaria et al. (2020)
(7) Delaria et al. (2018)
(8) Chaparro-Suarez et al. (2011)
(9) Breuninger et al. (2013)

Table S3: Calculated monthly nocturnal above-canopy $V_d(NO_2)$ at Harvard Forest using bulk-canopy $R_c(NO_2)$ computed from: (i) bottom-up estimates of component canopy surface resistances using surface-specific NO_2 uptake coefficients (Table 1) and relevant surface area scaling; (ii) r_{hyd} following Eq. (11) with top-down constraints on the surface area scaling term α (Section 3.3.3).

	Jan.	Feb.	March	April	May	June	July	Aug.	Sept.	Oct.	Nov.	Dec.
Canopy Conditions [a]												
T @ 15 m [°C]	-7.2	-6.2	-0.2	4.5	9.7	15	17	18	14	7.2	3.0	-2.0
RH @ 15 m [%]	82	73	79	72	79	88	89	88	91	85	84	79
LAI	0.83	0.83	0.83	0.88	2.3	4.0	4.2	4.2	3.9	2.5	1.1	0.83
u^* [m s^{-1}] [b]	0.57	0.62	0.59	0.51	0.47	0.42	0.38	0.38	0.41	0.45	0.57	0.60
Aerodynamic Res. [c]												
R_a(29 m) [s m^{-1}]	11.6	10.1	11.3	13.9	13.2	14.9	16.9	17.3	15.7	14.6	10.7	12.0
Quasi-Laminar Res. [c]												
R_b(NO2) [s m^{-1}]	14.0	12.1	12.8	14.9	14.8	16.4	17.8	16.7	16.3	15.4	12.6	12.5
Bottom-up $V_d(NO_2)$ [d]												
r_c, leaf [s m^{-1}]	3010	3010	2970	2870	1730	1020	973	990	1090	1620	2670	2980
r_c, bark [s m^{-1}]	756	708	712	706	683	607	620	632	666	712	707	729
r_a, canopy [s m^{-1}]	573	495	561	679	872	1180	1380	1390	1180	988	579	512
r_c, floor [s m^{-1}]	684	657	513	261	258	256	255	254	256	259	261	571
R_c, canopy [s m^{-1}]	395	359	350	339	312	279	292	291	301	326	300	356
R_c, canopy [s m^{-1}] [e]	541	490	471	455	411	368	385	382	394	429	391	480
V_d [cm s^{-1}]	0.25	0.28	0.29	0.29	0.32	0.35	0.33	0.33	0.32	0.30	0.33	0.28
V_d [cm s^{-1}] [e]	0.18	0.21	0.22	0.23	0.25	0.27	0.25	0.26	0.25	0.24	0.26	0.22
Top-down $V_d(NO_2)$ [f]												
$R_c = r_{hyd}$(α=1) [s m^{-1}]	719	773	864	1108	970	822	795	728	774	903	862	759
$R_c = r_{hyd}$(α=2) [s m^{-1}]	406	445	452	554	485	411	397	364	387	452	431	423
V_d (α=1) [cm s^{-1}]	0.13	0.13	0.12	0.1	0.11	0.12	0.12	0.13	0.13	0.11	0.12	0.13
V_d (α=2) [cm s^{-1}]	0.23	0.22	0.22	0.19	0.21	0.24	0.24	0.26	0.24	0.22	0.23	0.23

[a] T, RH, and u^* are nocturnal (2000–0400 LST) monthly medians from an hourly data set spanning 2000–2002.

[b] Periods of low turbulence ($u^* < 0.2$ m s^{-1}) were excluded from analysis (Section 2.2.2).

[c] Above-canopy aerodynamic resistance computed as $R_a(29m) = u\ (29\ m)/u^{*2}$; quasi-laminar boundary layer resistance R_b computed following Eq. (4).

[d] Bottom-up $V_d(NO_2)$ computed following Eq. (2), with R_c following Eq. (13). Component $r_c = 4/(\bar{v}_t\ \gamma\ \alpha)$, where uptake coefficients are from Table 1. The forest floor was assumed snow covered for months DJFM when T < 0 °C. Canopy component surface area scale factors where: $\alpha_{leaf} = [1\ (RH < 96\%)\ \text{or}\ 2\ (\text{RH} > 96\%)]DLAI + 2.7CAI$, where CAI = 0.83, and DLAI = LAI – CAI are the projected areas of coniferous needles and deciduous leaves; $\alpha_{bark} = \pi$STAI, where STAI = 0.9 is the projected area of tree branches; $\alpha_{floor} = 1$ as $\bar{\gamma}_{floor}$ and $\bar{\gamma}_{snow}$ from Table 1 are reported for planar surfaces. Note, NO_2 hydrolysis is assumed to occur on the stomatal surfaces of leaves (lower for deciduous and total for coniferous) at RH < 96% due to the presence of thin water films and on both upper and lower surfaces of deciduous leaves for RH > 96% (Section 3.3.4). In-canopy aerodynamic resistance (r_a) follows Zhang et al. (2003) $r_a = R_{ac0}\ LAI^{0.25}\ u^{*-2}$, where R_{ac0} are land type specific prescribed values.

[e] Computed with uptake to bark reduced by a factor of two (Section 3.3.4).

[f] Top-down $V_d(NO_2)$ computed following Eq. (2) and r_{hyd} following Eqs. (10–11). Note, snow is assumed present for months DJFM when T < 0 °C where $\bar{\gamma}_{snow} = 1.6 \times 10^{-5}$ is used for all available surface area for r_{hyd}, α = 1, and ½ of available surface area for r_{hyd}, α = 2.

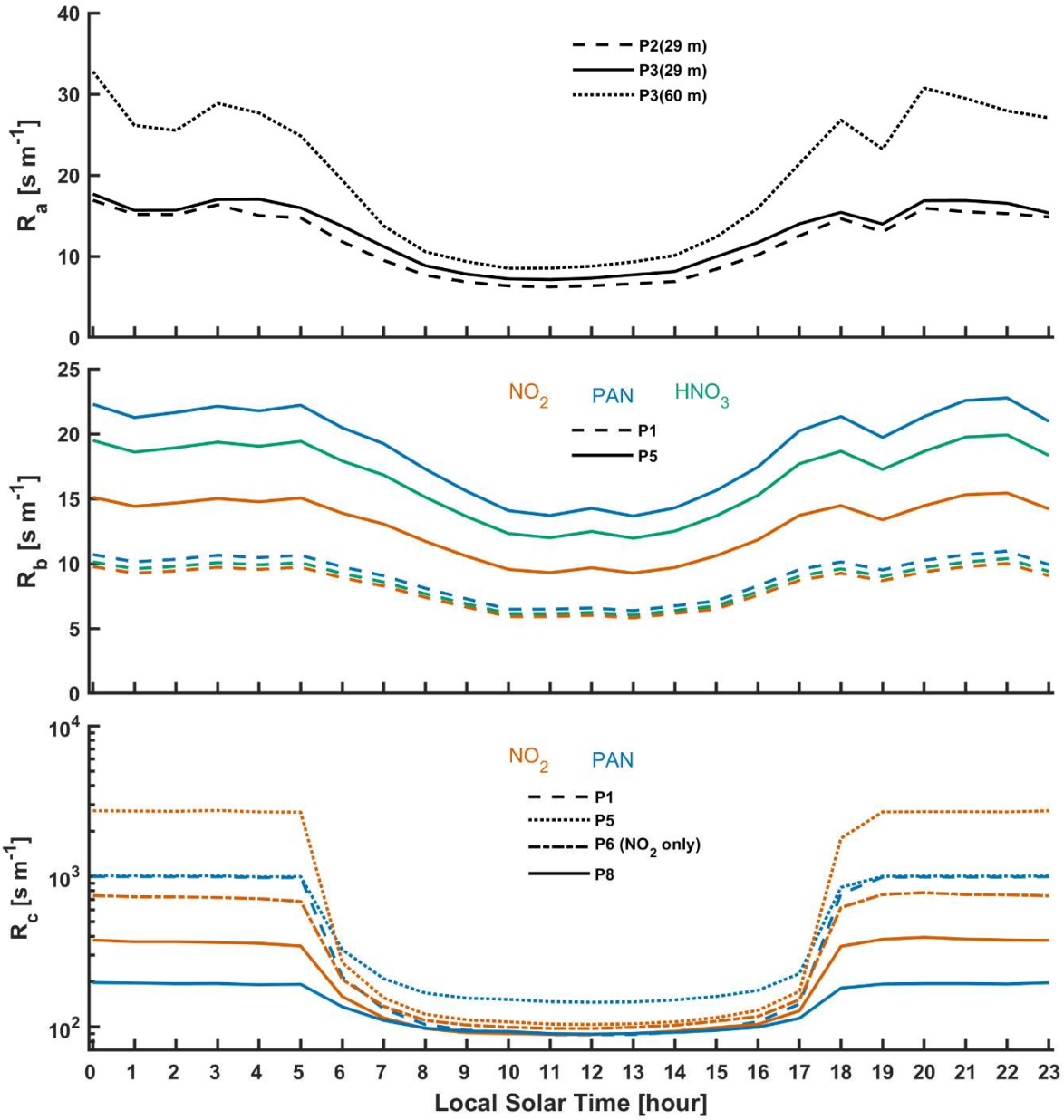

Figure S6: Median component resistances R_a, R_b, and R_c from parameterized deposition velocities for HNO_3, NO_2, and PAN over Harvard Forest. Aerodynamic resistance $\boldsymbol{R_a}$ is common to all species and depicted for parameterizations P2 and P3 computed from the 29 m or 60 m measurement height, as indicated. Quasi-laminar boundary layer resistance $\boldsymbol{R_b}$ is shown for all species according to parameterizations P1 and P5. Surface layer resistances $\boldsymbol{R_c}$ for NO_2 and PAN are depicted for parameterizations P1, P5, P6, and P8 (equivalent to P7 for NO_2; Table 2).

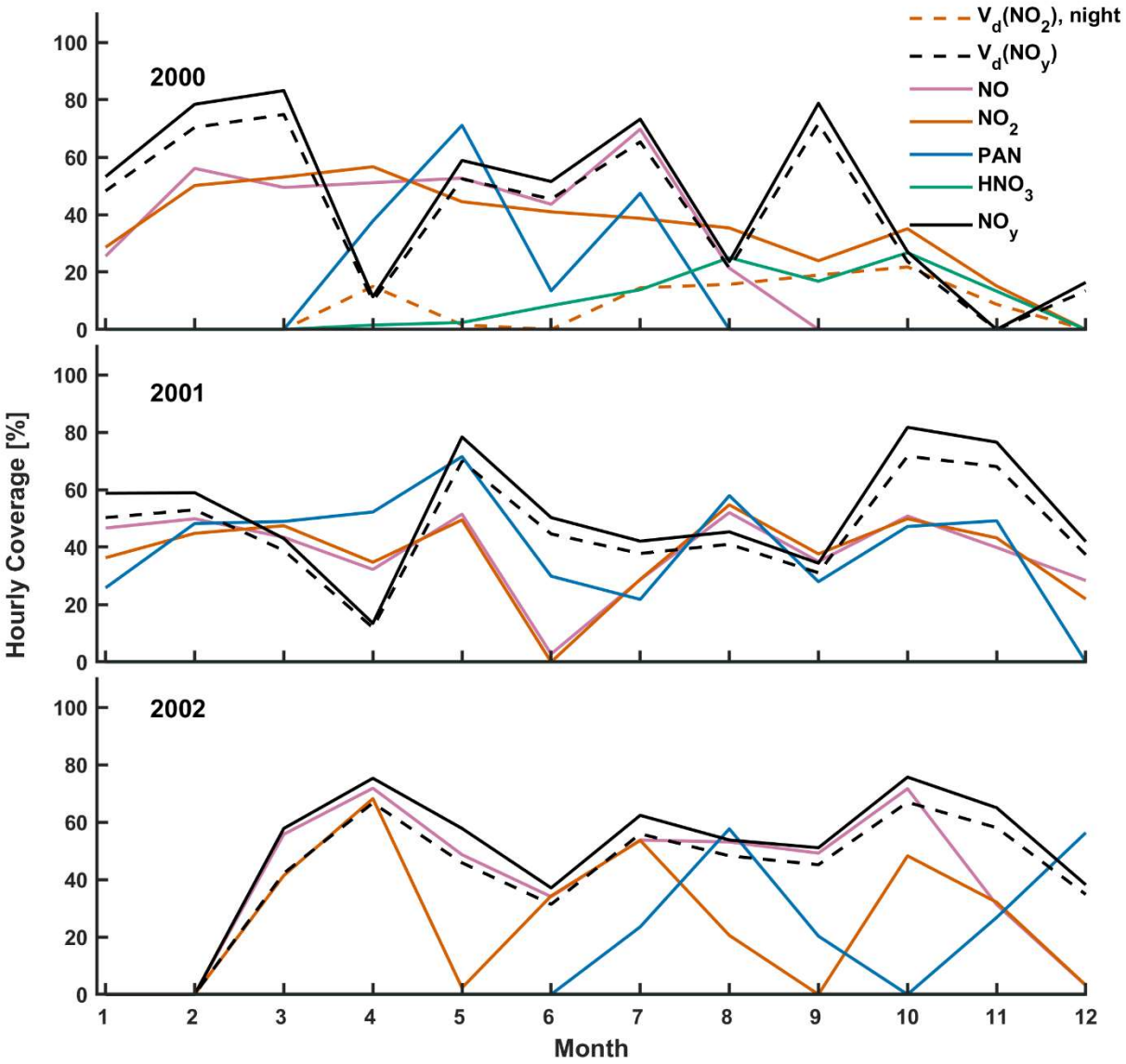

Figure S7: Hourly coverage of measured above-canopy trace gas concentrations and eddy covariance observed deposition velocities at Harvard Forest from 2000–2002. Measurements taken during conditions of low turbulence ($u_* < 0.2$ m s^{-1}) where omitted from analysis (Section 2.2.2).

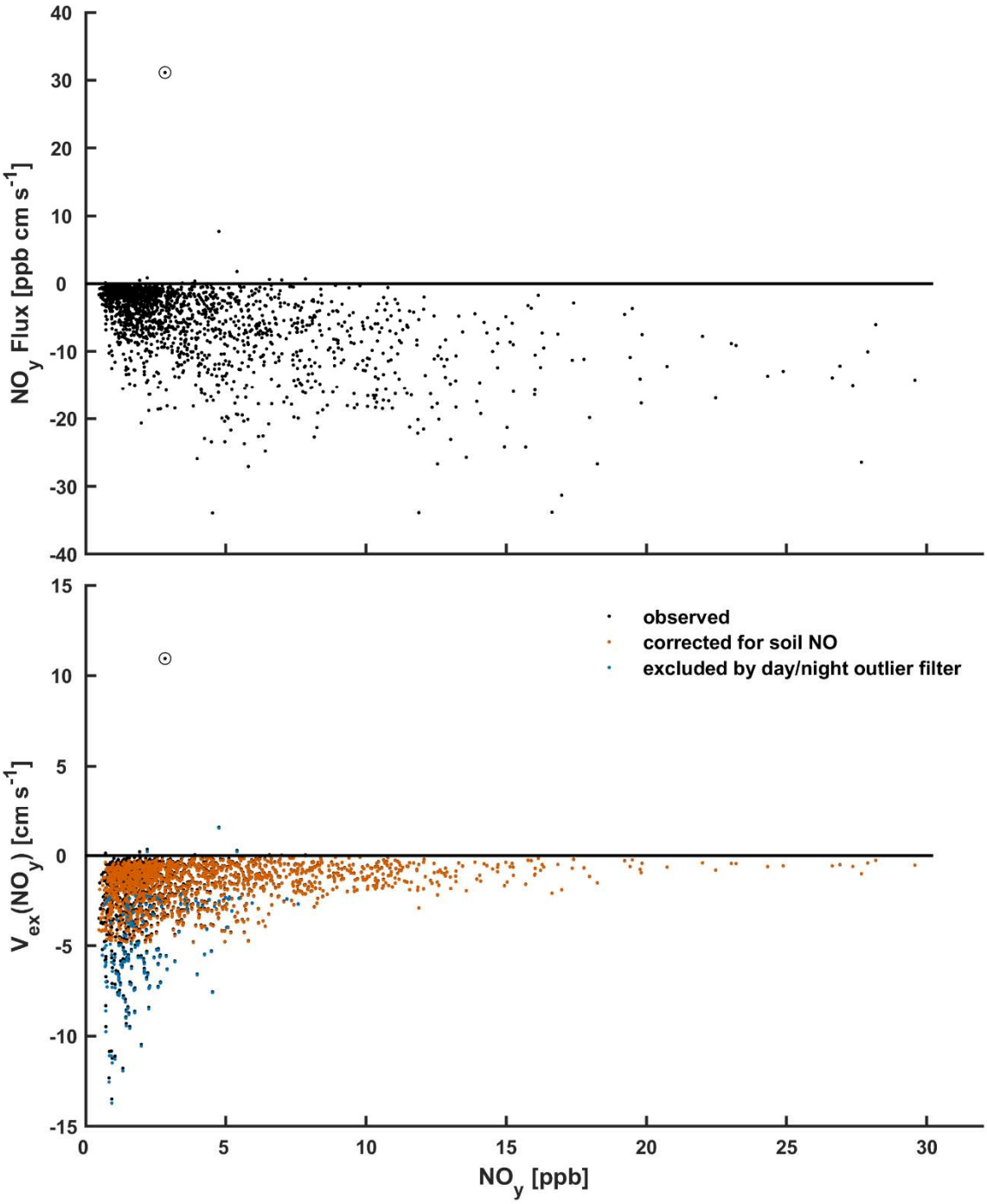

Figure S8: Hourly eddy covariance NO_y fluxes (**Top**) and resulting exchange velocities $V_{ex(NO_y)}$ (**Bottom**) as a function of NO_y concentration over Harvard Forest. These publicly available measurements (Horii, 2004) were made over an established mixed deciduous forest (Harvard Forest, MA, U.S.) from June–November 2000. Estimated above-canopy soil NO flux was subtracted from measured hourly NO_y fluxes in order to estimate $V_{ex(NO_y)}$ due to deposition (depicted as 'corrected for soil NO'). Data excluded by a day/night $V_{ex(NO_y)}$ outlier filter are shown in blue. Data points excluded from analysis based on visual inspection are circled. Hourly observations made under conditions of low turbulence ($u_* < 0.2$ m s^{-1}) were excluded from analysis (Section 2.2.2).

References

Ammann, M., Rössler, E., Strekowskit, R. and George, C.: Nitrogen dioxide multiphase chemistry: Uptake kinetics on aqueous solutions containing phenolic compounds, Phys. Chem. Chem. Phys., 7(12), 2513–2518, doi:10.1039/b501808k, 2005.

Ammann, M., Cox, R. A., Crowley, J. N., Jenkin, M. E., Mellouki, A., Rossi, M. J., Troe, J. and Wallington, T. J.: Evaluated kinetic and photochemical data for atmospheric chemistry: Volume VI - Heterogeneous reactions with liquid substrates, Atmos. Chem. Phys., 13(16), 8045–8228, doi:10.5194/acp-13-8045-2013, 2013.

Arnqvist, J. and Bergström, H.: Flux-profile relation with roughness sublayer correction, Q. J. R. Meteorol. Soc., 141(689), 1191–1197, doi:10.1002/qj.2426, 2015.

Bambauer, A., Brantner, B., Paige, M. and Novakov, T.: Laboratory Study of NO2 Reaction With Dispersed and Bulk Liquid Water, Atmosperic Environ., 28(20), 3225–3232, 1994.

Bang, J., Lee, D. H., Kim, S. K. and Kang, H.: Reaction of Nitrogen Dioxide with Ice Surface at Low Temperature (>170 K), J. Phys. Chem. C, 119(38), 22016–22024, doi:10.1021/acs.jpcc.5b05497, 2015.

Bannister, E. J., Jesson, M., Harper, N. J., Hart, K. M., Curioni, G. and Mackenzie, A. R.: Air-parcel residence times in a mature forest : observational evidence from a free-air CO 2 enrichment experiment, Atmos. Chem. Phys. Discuss., (May), 1–27, 2022.

Breuninger, C., Meixner, F. X. and Kesselmeier, J.: Field investigations of nitrogen dioxide (NO2) exchange between plants and the atmosphere, Atmos. Chem. Phys., 13(2), 773–790, doi:10.5194/acp-13-773-2013, 2013.

Bröske, R., Kleffmann, J. and Wiesen, P.: Heterogeneous conversion of NO2 on secondary organic aerosol surfaces: A possible source of nitrous acid (HONO) in the atmosphere?, Atmos. Chem. Phys., 3(3), 469–474, doi:10.5194/acp-3-469-2003, 2003.

Bryan, A. M., Bertman, S. B., Carroll, M. A., Dusanter, S., Edwards, G. D., Forkel, R., Griffith, S., Guenther, A. B., Hansen, R. F., Helmig, D., Jobson, B. T., Keutsch, F. N., Lefer, B. L., Pressley, S. N., Shepson, P. B., Stevens, P. S. and Steiner, A. L.: In-canopy gas-phase chemistry during CABINEX 2009: Sensitivity of a 1-D canopy model to vertical mixing and isoprene chemistry, Atmos. Chem. Phys., 12(18), 8829–8849, doi:10.5194/acp-12-8829-2012, 2012.

Burkhardt, J.: Hygroscopic particles on leaves: nutrients or desiccants?, Ecol. Monogr., 80(3), 369–399, 2010.

Burkhardt, J. and Gerchau, J.: Thin Water Films on Coniferous Needles, Atmosperic Environ., 28(12), 2001–2017, 1994.

Burkhardt, J. and Hunsche, M.: " Breath figures " on leaf surfaces — formation and effects of microscopic leaf wetness, Front. Plant Sci., 4(October), 1–9, doi:10.3389/fpls.2013.00422, 2013.

Burkhardt, J., Kaiser, H., Goldbach, H. and Kappen, L.: Measurements of electrical leaf surface conductance reveal recondensation of transpired water vapour on leaf surfaces, Plant, Cell Environ., 22(2), 189–196, doi:10.1046/j.1365-3040.1999.00387.x, 1999.

Burkhardt, J., Koch, K. and Kaiser, H.: Deliquescence of Deposited Atmospheric Particles on Leaf Surfaces, Air-Surface Exch. Gases Part., 1, 313–321, doi:10.1007/978-94-010-9026-1_31, 2001a.

Burkhardt, J., Kaiser, H., Kappen, L. and Goldbach, H. E.: The possible role of aerosols on stomatal conductivity for water vapour, Basic Appl. Ecol., 364, 351–364, 2001b.

Burkhardt, J., Zinsmeister, D., Grantz, D. A., Vidic, S. and Sutton, M. A.: Camouflaged as degraded wax : hygroscopic aerosols contribute to leaf desiccation , tree mortality , and forest decline Camouflaged as degraded wax : hygroscopic aerosols contribute to leaf desiccation , tree mortality , and forest decline, Environ. Res. Lett., 13(8), 085001, 2018.

Cellier, P. and Brunet, Y.: Flux-gradient relationships above tall plant canopies, Agric. For. Meteorol., 58, 93–117, 1992.

Chaparro-Suarez, I. G., Meixner, F. X. and Kesselmeier, J.: Nitrogen dioxide (NO2) uptake by vegetation controlled by atmospheric concentrations and plant stomatal aperture, Atmos. Environ., 45(32), 5742–5750, doi:10.1016/j.atmosenv.2011.07.021, 2011.

Cheung, J. L., Li, Y. Q., Boniface, J., Shi, Q., Davidovits, P., Worsnop, D. R., Jayne, J. T. and Kolb, C. E.: Heterogeneous Interactions of NO2 with Aqueous Surfaces, J. Phys. Chem. A, 104(12), 2655–2662, doi:10.1021/jp992929f, 2000.

Colussi, A. J. and Enami, S.: Detecting intermediates and products of fast heterogeneous reactions on liquid surfaces via online mass spectrometry, Atmosphere (Basel)., 10(2), doi:10.3390/atmos10020047, 2019.

Costa, J. M., Monnet, F., Jannaud, D., Leonhardt, N., Ksas, B., Reiter, I. M., Pantin, F. and Genty, B.: OPEN ALL NIGHT LONG : The Dark Side of Stomatal Control 1, Plant Physiol., 167, 289–294, doi:10.1104/pp.114.253369, 2015.

Delaria, E., Place, B., Liu, A. and Cohen, R.: Laboratory measurements of stomatal NO2 deposition to native California trees and the role of forests in the NOx cycle, Atmos. Chem. Phys., 20(2), 14023–14041, doi:10.5194/acp-2020-240, 2020.

Delaria, E. R. and Cohen, R. C.: A model-based analysis of foliar NOx deposition, Atmos. Chem. Phys., 20, 2123–2141, doi:10.5194/acp-20-2123-2020, 2020.

Delaria, E. R., Vieira, M., Cremieux, J. and Cohen, R. C.: Measurements of NO and NO2 exchange between the atmosphere and Quercus agrifolia, Atmos. Chem. Phys., 18(19), 14161–14173, doi:10.5194/acp-18-14161-2018, 2018.

Dyer, A. J.: A Review of Flux-Profile Relationships, Boundary-Layer Meteorol., 7, 363–372, 1974.

Farvardin, A., Isabel, A., Llorens, E., Garc, P., Scalschi, L. and Vicedo, B.: The Apoplast : A Key Player in Plant Survival same, Antioxidants, 6(604), doi:10.3390/antiox9070604, 2020.

Finlayson-Pitts, B. J.: Reactions at surfaces in the atmosphere: integration of experiments andtheory as necessary (but not necessarily sufficient) for predicting thephysical chemistry of aerosols, Phys. Chem. Chem. Phys., 11(36), 7759, doi:10.1039/b916865f, 2009.

Finlayson-Pitts, B. J., Wingen, L. M., Sumner, A. L., Syomin, D. and Ramazan, K. A.: The heterogeneous hydrolysis of NO2 in laboratory systems and in outdoor and indoor atmospheres: An integrated mechanism, Phys. Chem. Chem. Phys., 5(2), 223–242, doi:10.1039/B208564J, 2003.

Finnigan, J.: Turbulence in plant canopies, Annu. Rev. Fluid Mech., 35, 519–571, doi:10.2480/agrmet.20.1, 2000.

Finnigan, J. J., Shaw, R. H. and Patton, E. G.: Turbulence structure above a vegetation canopy, J. Fluid Mech., 637(May), 387–424, doi:10.1017/S0022112009990589, 2009.

Gallo, A., Farinha, A. S. F., Emwas, A. H., Santana, A., Nielsen, R. J., Goddard, W. A. and Mishra, H.: Reply to the 'Comment on "The chemical reactions in electrosprays of water do not always correspond to those at the pristine air–water interface"' by A. J. Colussi and S. Enami, Chem. Sci., 2019, 10, DOI: 10.1039/c9sc00991d, Chem. Sci., 10, 8256–8261, doi:10.1039/c9sc00991d, 2019a.

Gallo, A., Farinha, A. S. F., Dinis, M., Emwas, A. H., Santana, A., Nielsen, R. J., Goddard, W. A. and Mishra, H.: The chemical reactions in electrosprays of water do not always correspond to those at the pristine air-water interface, Chem. Sci., 10(9), 2566–2577, doi:10.1039/c8sc05538f, 2019b.

Garratt, J. R.: Surface influence on vertical profiles in the atmospheric near-surface layer, Q. J. R. Meteorol. Soc., 96, 211–255, 1980.

Garratt, J. R.: The atmospheric boundary layer, edited by J. . Houghton, M. J. Rycroft, and A. J. Dessler, Cambridge University Press., 1992.

Gerken, T., Chamecki, M. and Fuentes, J. D.: Air-Parcel Residence Times Within Forest Canopies, Bound. Layer Meteorol., 165, 29–54, 2017.

Grantz, D. A., Zinsmeister, D. and Burkhardt, J.: Ambient aerosol increases minimum leaf conductance and alters the aperture – flux relationship as stomata respond to vapor pressure deficit (VPD), New Phytol., 219, 275–286, doi:10.1111/nph.15102, 2018.

Grøntoft, T. and Raychaudhuri, M. R.: Compilation of tables of surface deposition velocities for O3, NO2 and SO2 to a range of indoor surfaces, Atmos. Environ., 38(4), 533–544, doi:10.1016/j.atmosenv.2003.10.010, 2004.

Gu, W., Cheng, P. and Tang, M.: Compilation and evaluation of gas phase diffusion coefficients of halogenated organic compounds, R. Soc. Open Sci., 5(7), doi:10.1098/rsos.171936, 2018.

Haghighi, E. and Or, D.: Linking evaporative fluxes from bare soil across surface viscous sublayer with the Monin-Obukhov atmospheric flux-profile estimates, J. Hydrol., 525, 684–693, doi:10.1016/j.jhydrol.2015.04.019, 2015.

Hanson, P. J., Rott, K., Taylor, G. E., Gunderson, C. A., Lindberg, S. E. and Ross-Todd, B. M.: NO2 Deposition to Elements Representative of a Forest Landscape, Atmos. Environ., 23, 1783–1794, 1989.

Harman, I. N. and Finnigan, J. J.: A simple unified theory for flow in the canopy and roughness sublayer, Boundary-Layer Meteorol., 123(2), 339–363, doi:10.1007/s10546-006-9145-6, 2007.

Holtslag, A. A. M. and Bruin, H. A. R.: Applied Modeling of the Nighttime Surface Energy Balance over Land, J. Appl. Meteorol., 27, 689–703, 1988.

Holtslag, A. A. M., De Bruijn, E. I. F. and Pan, H. L.: A High Resolution Air Mass Transformation Model for Short-Range Weather Forecasting, Mon. Weather Rev., 118, 1561–1575, 1990.

Horii, C. V., Munger, J. W., Wofsy, S. C., Zahniser, M., Nelson, D. and McManus, J. B.: Fluxes of nitrogen oxides over a temperate deciduous forest, J. Geophys. Res. D Atmos., 109(8), doi:10.1029/2003JD004326, 2004.

Horii, C. V., Munger, J. W., Wofsy, S. C., Zahniser, M., Nelson, D. and Mcmanus, J. B.: Atmospheric reactive nitrogen concentration and flux budgets at a Northeastern U . S . forest site, Agric. For. Meteorol., 133, 210–225, doi:10.1016/j.agrformet.2006.03.005, 2005.

Hudman, R. C., Moore, N. E., Mebust, A. K., Martin, R. V., Russell, A. R., Valin, L. C. and Cohen, R. C.: Steps towards a mechanistic model of global soil nitric oxide emissions: Implementation and space based-constraints, Atmos. Chem. Phys., 12(16), 7779–7795, doi:10.5194/acp-12-7779-2012, 2012.

Jacob, D. J. and Wofsy, S. C.: Budgets of reactive nitrogen, hydrocarbons, and ozone over the Amazon forest during the wet season, J. Geophys. Res., 95(D10), doi:10.1029/jd095id10p16737, 1990.

Kaimal, J. C. and Finnigan, J. .: Atmospheric Boundary Layer Flows, Their Structure and Measurement, Oxford University Press., 1994.

Karamchandani, P., Emery, C., Yarwood, G., Lefer, B., Stutz, J., Couzo, E. and Vizuete, W.: Implementation and refinement of a surface model for heterogeneous HONO formation in a 3-D chemical transport model, Atmos. Environ., 112, 356–368, doi:10.1016/j.atmosenv.2015.01.046, 2015.

Kinugawa, T., Enami, S., Yabushita, A., Kawasaki, M., Hoffmann, M. R. and Colussi, A. J.: Conversion of gaseous nitrogen dioxide to nitrate and nitrite on aqueous surfactants, Phys. Chem. Chem. Phys., 13(11), 5144–5149, doi:10.1039/c0cp01497d, 2011.

Kleffmann, J., Becker, K. H. and Wiesen, P.: Investigation of the heterogeneous NO2 conversion on perchloric acid surfaces, J. Chem. Soc. - Faraday Trans., 94(21), 3289–3292, doi:10.1039/a805440a, 1998.

Kurtenbach, R., Becker, K. H., Gomes, J. A. G., Kleffmann, J., Lörzer, J. C., Spittler, M., Wiesen, P., Ackermann, R., Geyer, A. and Platt, U.: Investigations of emissions and heterogeneous formation of HONO in a road traffic tunnel, Atmos. Environ., 35(20), 3385–3394, doi:10.1016/S1352-2310(01)00138-8, 2001.

Lamaud, E., Loubet, B., Irvine, M., Stella, P., Personne, E. and Cellier, P.: Partitioning of ozone deposition over a developed maize crop between stomatal and non-stomatal uptakes, using eddy-covariance flux measurements and modelling, Agric. For. Meteorol., 149(9), 1385–1396, doi:10.1016/j.agrformet.2009.03.017, 2009.

Langenberg, S., Carstens, T., Hupperich, D., Schweighoefer, S. and Schurath, U.: Technical note: Determination of binary gas-phase diffusion coefficients of unstable and adsorbing atmospheric trace gases at low temperature – arrested flow and twin tube method, Atmos. Chem. Phys., 20(6), 3669–3682, doi:10.5194/acp-20-3669-2020, 2020.

Lee, Y. N. and Schwartz, S. E.: Reaction kinetics of nitrogen dioxide with liquid water at low partial pressure, J. Phys. Chem., 85(7), 840–848, doi:10.1021/j150607a022, 1981.

Lerdau, M. T., Munger, J. W. and Jacob, D. J.: The NO2 flux conundrum, Science (80-.)., 289(5488), 2291–2293, doi:10.1126/science.289.5488.2291, 2000.

Martens, C., Shay, T. J., Mendlovitz, H. P., Matross, D. M., Saleska, S. R., Wofsy, S. C. and et al.: Radon fluxes in tropical forest ecosystems of Brazilian Amazonia : night-time CO 2 net ecosystem exchange derived from radon and eddy covariance methods, Glob. Chang. Biol., 10, 618–629, doi:10.1111/j.1529-8817.2003.00764.x, 2004.

Massman, W. J.: An evaluation of the regional acid deposition model surface module for ozone uptake at three sites in the San Joaquin Valley of California, J. Geophys. Res., 99(D4), 8281–8294, doi:10.1029/93JD03267, 1994.

Massman, W. J.: A review of the molecular diffusivities of H2O, CO2, CH4, CO, O3, SO2, NH3, N2O, NO, and NO2 in air, O2 and N2 near STP, Atmos. Environ., 32(6), 1111–1127, doi:10.1016/S1352-2310(97)00391-9, 1998.

Matthes, J., Munger, W. and Wofsy, S.: Biomass Inventories at Harvard Forest EMS Tower since 1993, Harvard Forest Data Archive: HF069 [data set], https://doi.org/10.6073/pasta/0292c5bdb53f80dffee596295cb080ca, 2024.

Mertes, S. and Wahner, A.: Uptake of nitrogen dioxide and nitrous acid on aqueous surfaces, J. Phys. Chem., 99(38), 14000–14006, doi:10.1021/j100038a035, 1995.

Min, K. E., Pusede, S. E., Browne, E. C., LaFranchi, B. W. and Cohen, R. C.: Eddy covariance fluxes and vertical concentration gradient measurements of NO and NO2 over a ponderosa pine ecosystem: Observational evidence for within-canopy chemical removal of NOx, Atmos. Chem. Phys., 14(11), 5495–5512, doi:10.5194/acp-14-5495-2014, 2014.

Mölder, M., Grelle, A., Lindroth, A. and Halldin, S.: Flux-profile relationships over a boreal forest - Roughness sublayer corrections, Agric. For. Meteorol., 98–99, 645–658, doi:10.1016/S0168-1923(99)00131-8, 1999.

Monin, A. S. and Obukhov, A. M.: Basic laws of turbulent mixing in the surface layer of the atmosphere, Contrib. Geophys. Inst. Acad. Sci. USSR, 151, 163–187, 1954.

Motai, A., Yamazaki, M., Muramatsu, N., Watanabe, M. and Izuta, T.: Submicron ammonium sulfate particles deposited on leaf surfaces of a leafy vegetable (Komatsuna , Brassica rapa L . var . perviridis) are taken up by leaf and enhance nocturnal leaf conductance, Atmosperic Environ., 187(May), 155–162, doi:10.1016/j.atmosenv.2018.05.064, 2018.

Msibi, I. M., Shi, J. P. and Harrison, R. M.: Accommodation coefficient for trace gas uptake using deposition profile measurement in an annular reactor, J. Atmos. Chem., 17(4), 339–351, doi:10.1007/BF00696853, 1993.

Munger, J. W., Wofsy, S. C., Bakwin, P. S., Fan, S., Goulden, M. L., Daube, B. C., Goldstein, A. H., Moore, K. E. and Fitzjarrald, D. R.: Atmospheric deposition of reactive nitrogen oxides and ozaone in a temperate deciduos forest and a subartic woodland 1. measurements and mechanisms, J. Geophys. Res., 101, 12639–12657, 1996.

Murdachaew, G., Varner, M. E., Phillips, L. F., Finlayson-Pitts, B. J. and Gerber, R. B.: Nitrogen dioxide at the air-water interface: Trapping, absorption, and solvation in the bulk and at the surface, Phys. Chem. Chem. Phys., 204–212, doi:10.1039/c2cp42810e, 2012.

Neirynck, J. and Ceulemans, R.: Bidirectional ammonia exchange above a mixed coniferous forest, Environ. Pollut., 154(3), 424–438, doi:10.1016/j.envpol.2007.11.030, 2008.

Nemitz, E., Sutton, M. A., Schjoerring, J. K., Husted, S. and Paul Wyers, G.: Resistance modelling of ammonia exchange over oilseed rape, Agric. For. Meteorol., 105(4), 405–425, doi:10.1016/S0168-1923(00)00206-9, 2000.

Nguyen, T. B., Crounse, J. D., Teng, A. P., St. Clair, J. M., Paulot, F., Wolfe, G. M. and Wennberg, P. O.: Rapid deposition of oxidized biogenic compounds to a temperate forest, Proc. Natl. Acad. Sci., 112(5), E392–E401, doi:10.1073/pnas.1418702112, 2015.

Nobel, P. S.: Physicochemical and Environmental Plant Physiology, Fourth Edi., Elsevier., 2009.

Nobel, P. S., Zaragoza, L. J. and Smith, W. K.: Relation between Mesophyll Surface Area, Photosynthetic Rate, and Illumination Level during Development for Leaves of Plectranthus parviforus Henckel, Plant Physiol., 55, 1067–1070, 1975.

Novakov, T.: Laboratory Study of NO2 Reaction with Dispersed and Bulk Liquid Water--Author's Reply, Atmosperic Environ., 29(18), 2559–2560, 1995.

Panofsky, H. A.: Determination of stress from wind and temperature measurements, Q. J. R. Meteorol. Soc. Soc., 89(379), 85–97, 1963.

Pariyar, S., Eichert, T., Goldbach, H. E., Hunsche, M. and Burkhardt, J.: The exclusion of ambient aerosols changes the water relations of sunflower (Helianthus annuus) and bean (Vicia faba) plants, Environ. Exp. Bot., 88, 43–52, doi:10.1016/j.envexpbot.2011.12.031, 2013.

Physick, W. L. and Garratt, J. R.: Incorporation of a High-Roughness Lower Boudnary into a Mesoscale Model for Studies of Dry Deposition over Complex Terrain, Boundary-Layer Meteorol., 74, 55–71, 1995.

Plake, D., Stella, P., Moravek, A., Mayer, J. C., Ammann, C., Held, A. and Trebs, I.: Comparison of ozone deposition measured with the dynamic chamber and the eddy covariance method, Agric. For. Meteorol., 206, 97–112, doi:10.1016/j.agrformet.2015.02.014, 2015.

Ramge, P., Badeck, F. -W, PLÖCHL, M. and KOHLMAIER, G. H.: Apoplastic antioxidants as decisive elimination factors within the uptake process of nitrogen dioxide into leaf tissues, New Phytol., 125(4), 771–785, doi:10.1111/j.1469-8137.1993.tb03927.x, 1993.

Raupach, M. R., Finnigan, J. J. and Brunet, Y.: Coherent eddies and turbulence in vegetation canopies: the mixing-layer analogy, Boundary-Layer Meteorol., 78(3–4), 351–382, doi:10.1007/BF00120941, 1996.

de Ridder, K.: Bulk transfer relations for the roughness sublayer, Boundary-Layer Meteorol., 134(2), 257–267, doi:10.1007/s10546-009-9450-y, 2010.

Rondón, A., Johansson, C. and Granat, L.: Dry Deposition of Nitrogen Dioxide and Ozone to Coniferous Forests, J. Geophys. Res., 98, 5159–5172, 1993.

Rovelli, G., Jacobs, M. I., Willis, M. D., Rapf, R. J., Prophet, A. M. and Wilson, K. R.: A critical analysis of electrospray techniques for the determination of accelerated rates and mechanisms of chemical reactions in droplets, Chem. Sci., 11(48), 13026–13043, doi:10.1039/d0sc04611f, 2020.

Schwartz, S. E. and Lee, Y. N.: Laboratory Study of NO2 Reaction with Dispersed and Bulk Liquid Water, Atmosperic Environ., 29(8), 2557–2559, 1995.

Sellers, P. J., Mintz, Y. and Dalcher, A.: A Simple Biosphere Model (SiB) for Use within General Circulation Models, J. Atmos. Sci., 43, 505–531, 1986.

Simpson, I. J., Thurtell, G. W., Neumann, H. H., Den Hartog, G. and Edwards, G. C.: The validity of similarity theory in the roughness sublayer above forests, Boundary-Layer Meteorol., 87(1), 69–99, doi:10.1023/A:1000809902980, 1998.

Spataro, F. and Ianniello, A.: Sources of atmospheric nitrous acid: State of the science, current research needs, and future prospects, J. Air Waste Manage. Assoc., 64(11), 1232–1250, doi:10.1080/10962247.2014.952846, 2014.

Stella, P., Kortner, M., Ammann, C., Foken, T., Meixner, F. X. and Trebs, I.: Measurements of nitrogen oxides and ozone fluxes by eddy covariance at a meadow: Evidence for an internal leaf resistance to NO2, Biogeosciences, 10(9), 5997–6017, doi:10.5194/bg-10-5997-2013, 2013.

Stocker, D. W., Zeller, K. F. and Stedman, D. H.: O3 and NO2 fluxes over snow measured by eddy correlation, Atmos. Environ., 29(11), 1299–1305, doi:10.1016/1352-2310(94)00337-K, 1995.

Stroud, C., Makar, P., Karl, T., Guenther, A., Geron, C., Turnipseed, A., Nemitz, E., Baker, B., Potosnak, M. and Fuentes, J. D.: Role of canopy-scale photochemistry in modifying biogenic-atmosphere exchange of reactive terpene species : Results from the CELTIC field study, , 110, 1–14, doi:10.1029/2005JD005775, 2005.

Su, H., Cheng, Y., Oswald, R., TBehrendt, T., Trebs, I., Meixner, F. X., Andreae, M. O., Cheng, P., Zhang, Y. and Poschl, U.: Soil Nitrite as a Source of Atmospheric HONO and PH Radicals, Science (80-.)., 333(September), 1616–1618, 2011.

Tang, M. J., Cox, R. A. and Kalberer, M.: Compilation and evaluation of gas phase diffusion coefficients of reactive trace gases in the atmosphere: Volume 1. Inorganic compounds, Atmos. Chem. Phys., 14(17), 9233–9247, doi:10.5194/acp-14-9233-2014, 2014.

Tang, M. J., Shiraiwa, M., Pöschl, U., Cox, R. A. and Kalberer, M.: Compilation and evaluation of gas phase diffusion coefficients of reactive trace gases in the atmosphere: Volume 2. Diffusivities of organic compounds, pressure-normalised mean free paths, and average Knudsen numbers for gas uptake calculations, Atmos. Chem. Phys., 15(10), 5585–5598, doi:10.5194/acp-15-5585-2015, 2015.

Teklemariam, T. A. and Sparks, J. P.: Leaf fluxes of NO and NO2 in four herbaceous plant species: The role of ascorbic acid, Atmos. Environ., 40(12), 2235–2244, doi:10.1016/j.atmosenv.2005.12.010, 2006.

Thoene, B., Rennenberg, H. and Weber, P.: Absorption of atmospheric NO2 by spruce (Picea abies) trees: II. Parameterization of NO2 fluxes by controlled dynamic chamber experiments, New Phytol., 134(2), 257–266, doi:10.1111/j.1469-8137.1996.tb04630.x, 1996.

Toyota, K., Dastoor, A. P. and Ryzhkov, A.: Parameterization of gaseous dry deposition in atmospheric chemistry models: Sensitivity to aerodynamic resistance formulations under statically stable conditions, Atmos. Environ., 147, 409–422, doi:10.1016/j.atmosenv.2016.09.055, 2016.

Trumbore, S. E., Keller, M., Wofsy, S. C. and DA Costa, J. M.: Measurements of Soil and Canopy Exchange Rates in the Amazon Rain Forest using 22Rn, J. Geophsical Res., 95, 16865–16873, 1990.

Wang, W., Ganzeveld, L., Rossabi, S., Hueber, J. and Helmig, D.: Measurement report: Leaf-scale gas exchange of atmospheric reactive trace species (NO2, NO, O3) at a northern hardwood forest in Michigan, Atmos. Chem. Phys., 20(19), 11287–11304, doi:10.5194/acp-20-11287-2020, 2020.

Wang, Y., Jacob, J. and Logan, A.: Global simulation of tropospheric O3-NOx-hydrocarbon chemistry: 1. Model Formulation, J. Geogr. Res., 103, 10713–10725, 1998.

Wen, D., Zhang, L., Lin, J. C., Vet, R. and Moran, M. D.: An evaluation of ambient ammonia concentrations over southern Ontario simulated with different dry deposition schemes within STILT-Chem v0.8, Geosci. Model Dev., 7(3), 1037–1050, doi:10.5194/gmd-7-1037-2014, 2014.

Wentworth, G. R., Murphy, J. G., Gregoire, P. K., Cheyne, C. A. L., Tevlin, A. G. and Hems, R.: Soil-atmosphere exchange of ammonia in a non-fertilized grassland: Measured emission potentials and inferred fluxes, Biogeosciences, 11(20), 5675–5686, doi:10.5194/bg-11-5675-2014, 2014.

Wenzel, A., Kalthoff, N. and Horlacher, V.: On the profiles of wind velocity in the roughness sublayer above a coniferous forest, Boundary-Layer Meteorol., 84(2), 219–230, doi:10.1023/A:1000444911103, 1997.

Wolfe, D. E.: Boulder Atmospheric Observatory: 1977–2016: The End of an Era and Lessons Learned, Bull. Am. Meteorol. Soc., 99(7), 1345–1358, doi:10.1175/BAMS-D-17-0054.1, 2018.

Yabushita, A., Enami, S., Sakamoto, Y., Kawasaki, M., Hoffmann, M. R. and Colussi, A. J.: Anion-catalyzed dissolution of NO2 on aqueous microdroplets, J. Phys. Chem. A, 113(17), 4844–4848, doi:10.1021/jp900685f, 2009.

Yienger, J. and Levy, H.: Empirical model of global soil-biogenic NOx emissions, J. Geogr. Res., 100, 11447–11464, 1995.